

Highly Efficient Cellular Acoustic Absorber of Graphene Ultrathin Drums

Kai Pang, Xiaoting Liu, Jintao Pang, Akram Samy, Jin Xie, Yingjun Liu,* Li Peng,* Zhen Xu,* and Chao Gao*

Atomically thin 2D graphene sheets exhibit unparalleled in-plane stiffness and large out-of-plane elasticity, thereby providing strong mechanical resonance for nanomechanical devices. The exceptional resonance behavior of ultrathin graphene, which promises the fabrication of superior acoustic absorption materials, however, remains unfulfilled for the lack of applicable form and assembly methods. Here, a highly efficient acoustic absorber is presented, wherein cellular networks of ultrathin graphene membranes are constructed into polymer foams. The ultrathin graphene drums exhibit strong resonances and efficiently dissipate sound waves in a broad frequency range. A record specific noise reduction coefficient (51.3 at 30 mm) is achieved in the graphene-based acoustic absorber, fully realizing the superior resonance properties of graphene sheets. The scalable method facilely transforms commercial polymer foams to superior acoustic absorbers with a $\approx 320\%$ enhancement in average absorption coefficient across wide frequencies from 200 to 6000 Hz. The graphene acoustic absorber offers a convenient method to exploit the extraordinary resonance properties of 2D sheets, opening extensive new applications in noise protection, building design, instruments and acoustic devices.

1. Introduction

Atomically thin graphene sheets intrinsically possess unparalleled in-plane stiffness but display large out-of-plane deformation under mechanical actuation,^[1,2] thereby exhibiting rich fascinating vibrational characteristics, enabling important emerging applications in nanomechanical devices, such as ultrasensitive mass sensor,^[3–5] broadband loudspeaker,^[6] and oscillators.^[7] The ultrathin graphene sheets should become an ideal candidate material for fabricating good acoustic absorbers with extraordinary efficiency. In principle, the strong resonant effect of graphene can efficiently dissipate the sound vibration and retard its propagation, especially for the low-frequency sound. To pursue high sound absorption, the forced resonance of membranes has been utilized in ultrathin metasurface resonators,^[8–10] decorated membrane resonators,^[11,12] metamaterials,^[13,14] and micro-perforated panels.^[15–18] This mechanism is replacing the linear response of frictional damping and wave velocity in pores of conventional materials,^[11] overcoming the confined low-frequency sound attenuation. As to the thickness limit, graphene sheets with nonlinear damping behavior^[19] can reasonably be harnessed to achieve new breakthrough in sound absorption, to meet the increasingly high requirements of acoustic protection in human hearing healthy, chips, and architectural design.^[20]

Graphene-based materials have been attempted to enhance acoustic absorption performances, however, unfulfilled its great theoretic expectations to achieve the disruptive improvements. Previously, two basic assembly forms of graphene have been proposed for acoustic absorbers: polymer-graphene composite foams^[21–24] and graphene-based foams.^[25,26] In the former polymer-graphene composite foams, graphene sheets were covered on polymer frameworks by dispersion infiltration. In this process, the surface tensions inevitably cause the collapse and aggregation of graphene sheets, which defied the ultrathin thickness of self-standing graphene drums. The resultant thick graphene drums with high bending rigidity greatly depressed the resonance effect and only achieved negligible enhancement in acoustic absorption.^[21–24] As to the other neat graphene foams, despite a favorable acoustic absorption efficiency,

K. Pang, X. Liu, Y. Liu, L. Peng, Z. Xu, C. Gao
MOE Key Laboratory of Macromolecular Synthesis and Functionalization
International Research Center for X Polymers
Department of Polymer Science and Engineering
Zhejiang University
38 Zheda Road, Hangzhou 310027, China
E-mail: yingjunliu@zju.edu.cn; l-peng@zju.edu.cn; zhenxu@zju.edu.cn;
chaogao@zju.edu.cn

J. Pang, J. Xie
The State Key Laboratory of Fluid Power and Mechatronic Systems
Zhejiang University
38 Zheda Road, Hangzhou 310027, China

A. Samy
Department of Civil Engineering and Architecture
Zhejiang University
Hangzhou 310058, China

Y. Liu
Shanxi-Zheda Institute of Advanced Materials and Chemical Engineering
Taiyuan 030000, China

C. Gao
Graphene Industry and Engineering Research Institute
Xiamen University
Xiamen 361005, China

 The ORCID identification number(s) for the author(s) of this article can be found under <https://doi.org/10.1002/adma.202103740>.

DOI: 10.1002/adma.202103740

their poor structural integrity^[27] not only limits the large-scale production but also generates sheets slippage with sound wave propagating which caused low-efficient resonance absorption. To date, the realization of high-efficient graphene acoustic absorber to exploit the superior resonance effect of graphene remains challenged by the lack of appropriate assembly forms and available processing methods.

Here, we report a cellular acoustic absorber with ultra-high efficiency in acoustic absorption. The graphene acoustic absorber is integrated by self-standing ultrathin graphene drums and cellular polymer microframes by the hydroplastic foaming (HPF) method. The achieved ultrathin thickness of graphene drums allows large out-of-plane resonance in the wide frequency range and serves as intrinsic elements to dissipate sound transport. The synergistic dissipation of ultrathin graphene drums and porous cavity contributes to the remarkable enhancement by $\approx 320\%$ of the average absorption coefficient extending from 200 to 6000 Hz. The specific noise reduction coefficient (NRC) is superior over many conventional and advanced sound absorbers ever achieved. The graphene acoustic absorber is applied in prototype tests to reach $\approx 90\%$ attenuation rate of sound, promising wide acoustic engineering applications from noise protection, instruments to building design and acoustic devices.

2. Result and Discussion

We proposed a multiscale structural model of acoustic absorber to fully harness the strong resonant merits of ultrathin graphene sheets. The architecture consists of self-standing ultrathin graphene drums and cellular polymer frameworks (Figure 1A). The floating graphene membranes cover polymeric trusses and act as acoustic resonance drums, forming a 3D framework to attenuate sound propagation. The proposed acoustic absorber includes two major work mechanisms,^[8,28] that are forced resonance of graphene drums and friction damping in pores. As to the first mechanism, the incident sound wave compels strong resonance of graphene drums and the propagation energy is dissipated stepwise by multiple drums along the pathway across the 3D framework, resulting in that only a small amount of sound can leak out (Figure 1B). At the same time, the compartment pores cause air vibration and frictional damping to absorb sound, similar to the conventional porous acoustic absorption materials.^[29] The dual mechanisms ensure the high efficiency in absorbing acoustic sound to achieve the superior absorbers of sound.

The challenging ultrathin thickness of self-standing graphene drums in our proposed absorber is realized by HPF method^[27] (Figure 2A), which turns thick graphene oxide (GO)

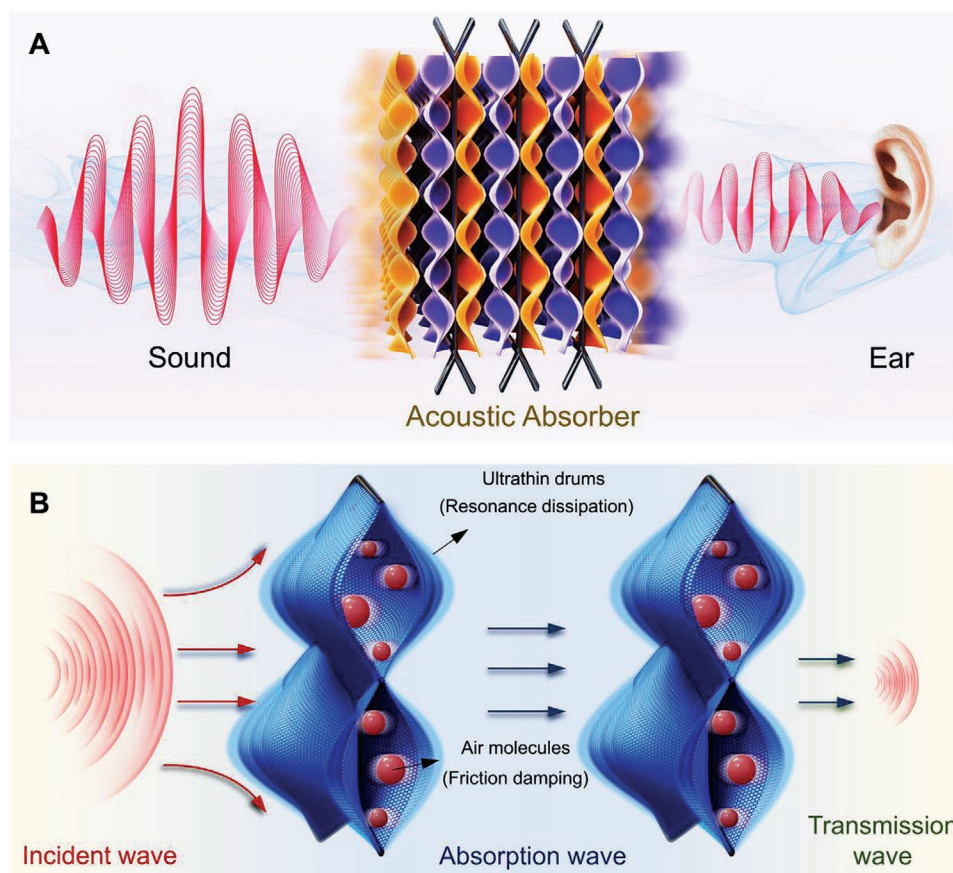


Figure 1. A) The proposed structure model of graphene-based, which includes the polymer porous motif and self-standing ultrathin graphene membranes. B) The multiple mechanisms of the graphene-based absorber to achieve superior absorption by the resonance of ultrathin graphene and air friction damping in the pores.

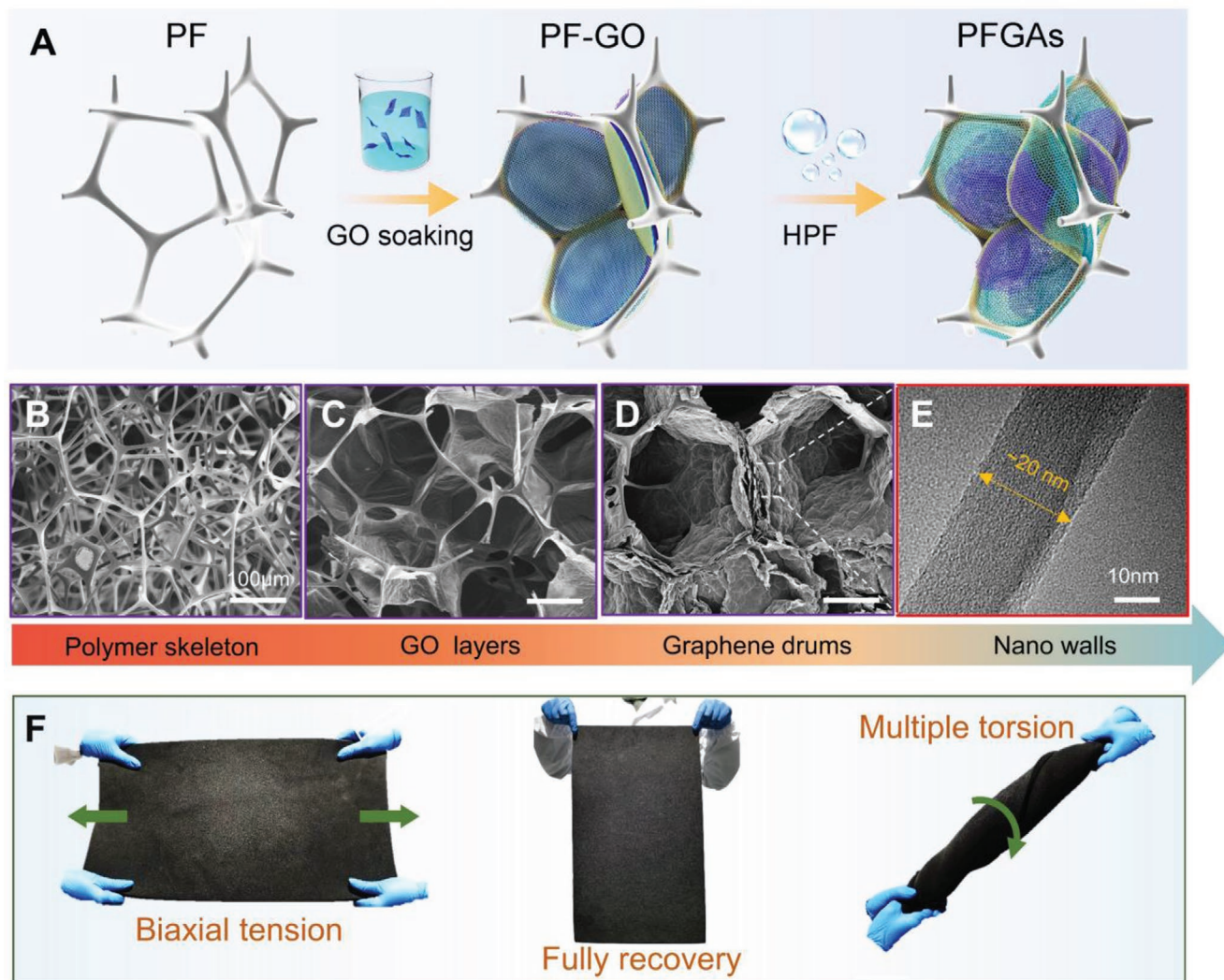


Figure 2. A–D) Representative diagram of the fabrication of PFGA (A) and corresponding SEM images of PF (B), PF-GO (C), and PFGA (D). E) The HRTEM image of graphene nanowalls in PFGA. F) The robust PFGA biaxial tension and multiple torsion.

membranes into porous aerogels with ultrathin walls. We first coated GO sheets onto the hexagonal polymer skeleton by facile dipping and GO sheets cannot form integrate self-standing membranes until reach a certain thickness (Figure 2B,C). The large thickness threshold of coated GO membranes is determined by the strong capillary force during dipping and drying, which forces the collapse of thin GO membranes because of their low bending rigidity. As in previous tries, self-standing GO membranes were coated into a polymer foam (PFGO) but with large thickness (Figure S2, Supporting Information), resulting in negligible enhancement in acoustic absorption.^[21,22] We supplemented HPF method to turn the thick GO solid membranes into a graphene aerogel (GA) with highly porous structure, creating ultrathin acoustic drums in the PF framework to form PFGA as an acoustic absorber.

In the HPF method, the water intercalation provides plasticity of GO membranes and enables the following bubbles foaming to form continuous graphene nanofilms without breakages. After plastic foaming, thick solid membranes

become highly porous but maintain the structural integration to cross over $\approx 100 \mu\text{m}$ (Figure 2D and Figure S3, Supporting Information). TEM analysis showed that the thickness of foamed walls reaches an ultrathin range down to $\approx 20 \text{ nm}$ (Figure 2E), which seems impossible to be realized by facile coating. The density and thickness of graphene drums can be controlled by the coating concentration ($1\text{--}10 \text{ mg mL}^{-1}$) of stock GO ink (Figure S3, Supporting Information) and foaming parameters such as foaming time and foaming reagent concentration^[27] (Figures S4–S7, Supporting Information). Figure S4, Supporting Information, demonstrated that the wall thickness became thinner and then thicker with the increase of foaming reagent concentration. On the other side, the pore size of GAs tends to decrease and then increase as the concentration increases (Figure S5, Supporting Information). Distinct from our previous work,^[27] the non-monotonic evolution of wall thickness and pore size is caused by the self-standing GO laminates that anchored on PF frameworks. At higher foaming reagent concentration (N_2H_4 solution of 50 wt%), GO laminate

is too thin to keep self-standing and detach from polymer trusses to stack to thicker walls and smaller pores. Besides, the pore size of GAs for PFGA can be controlled by the foaming time, representing a tendency to grow rapidly and then slowly (Figures S6 and S7, Supporting Information). Through these controlling steps, the maximum density of the graphene-based foam (PFGA) was only 11 mg cm^{-3} (Figure S8, Supporting Information), still holding higher porosity than most conventionally acoustic materials.^[29–31]

Our method is facile enough to prepare graphene-based acoustic absorber in a large scale but without the energy and time burden of using freeze-drying to strive the ultrathin thickness of graphene sheets in aerogels.^[32,33] This method facilely turns cheap commercial polymer sponges into high-quality acoustic absorbers, as shown in graphene-based acoustic absorber with an area of nearly one square meter (Figure 2F). Different from the fragile freeze-dried GAs, our prepared graphene-based acoustic absorber exhibited superior mechanical robustness, inheriting from the continuous face-to-face connection of plastic foaming skeleton. This structural robustness has been exhibited by the neat GAs by HPF previously.^[27] The graphene-based acoustic absorber maintained the structural integrity after severe deformations, such as biaxial tension and multiple torsion, similarly holding the remarkably mechanical stability as neat sponges (Figure 2F and Figure S9, Supporting Information). As expected, the embedding of GO sheets into PF framework can increase the modulus but decrease the elongation at break (Figure S10, Supporting Information). Beyond the ordinary properties of polymer sponges, graphene-based acoustic absorber exhibits rich functionalities to including super-hydrophobicity, high electrical conductivity (Figure S11, Supporting Information), and the greatly enhanced acoustic absorption ability. For example, graphene-based acoustic absorbers increased water contact angles from $\approx 0^\circ$ to 153° with the increased graphene content (Figure S11A,B, Supporting Information) and a maximum electrical conductivity of $\approx 4 \text{ S m}^{-1}$ (Figure S11C, Supporting Information).

We adopt suspended graphene nanofilms as structural model to verify the indispensable factor of ultrathinness of damping drums for acoustic absorption by resonance experiment and theoretical analysis. Self-standing graphene nanofilms with thickness from 20 to 320 nm were prepared by vacuum filtration and chemical reduction (Figure 3A–C). The semitransparent appearance demonstrated their ultrathin nature, which confirmed by the height measurement (for instance, $\approx 20 \text{ nm}$). Graphene nanofilms are mechanically strong enough to cross over a large spanning up to millimeters ($\approx 3 \text{ mm}$ in Figure 3A,B). We further fabricated piezoelectric resonance devices of self-standing graphene nanofilms as shown in Figure 3D. On these devices, we can study the thickness-dependent resonance behavior of graphene nanofilms.

We found that the thinner graphene nanofilm exhibits stronger resonant effect (Figure 3D–F). We employed flexible piezoelectric transducer (PZT) of polytetrafluoroethylene (PVDF) film as hollow substrate (Figure 3D), to simulate the sound frequency from 200 to 6000 Hz. The generated resonance was monitored by laser vibrometer. At a single-frequency input of 200 Hz, thinner graphene membrane exhibited larger

out-of-plane displacement, increased monotonically from $0.78 \text{ }\mu\text{m}$ for 320 nm thickness to $14.59 \text{ }\mu\text{m}$ (≈ 18.7 -fold) for 20 nm (Figure 3E). Thick graphene membrane (e.g., 320 nm) has poor resonance response and even suppresses the resonance of substrate, resulting the lower vibrational amplitude than the original PZT film. We also observed the same trend at the high-frequency input of 6000 Hz (Figure S12A, Supporting Information).

Beyond single-frequency sound source, the thickness dependence of resonance extends to a broad frequency range from 200 to 6000 Hz (Figure 3F and Figure S12B, Supporting Information). In the range of 200–2000 Hz, the 20 nm-thick membrane exhibited a full spectrum enhancement of resonance, especially prominent at several centers of 475, 525, 1547, 1800, and 1852 Hz. As a comparison, the 40 nm thick membrane had prominent enhancement at two centers of 950 and 1800 Hz, and 320 nm thick membrane behaved inactive as substrate. The spectrum scanning in 200–6000 Hz range demonstrated that the enhancement of 20 nm ultrathin graphene membranes mainly occurred at a frequency range of 200–2000 Hz (Figure 3F). It is shown that the thinner graphene nanofilm with lower bending rigidity has more sensitive resonance modes in low-frequency regime, which is in consistent with previous reports.^[11,28] Overall, the average resonance in the broad frequency range is gradually enhanced by thinning graphene nanofilm (Figure S12B, Supporting Information), justifying our structural design of ultrathin graphene drum to realize strong resonance for PFGA. Besides, it can be concluded the thicker graphene membrane (Figure 3F) resulted the shift of resonance peaks towards the high-frequency region, which was consistent with the theoretical prediction.^[2] We further studied the thickness-dependent resonance behavior by finite element analysis (FEA) and found that the lower bending rigidity of thinner nanofilm facilitates the conversion of external stimulus to resonant deformation (Figure 3G and Movie S1, Supporting Information). The numerical results showed that the out-of-plane amplitude increases monotonically as thickness decreases (Figure 3G,H), agreeing well with the experimental results.

As expected in the structural design and model validation, graphene-based absorber with ultrathin graphene drums showed excellent sound-absorption performance, in a broad frequency range of 200–6000 Hz (Figure 4). Figure 4A shows that the absorption coefficient of PFGA is much higher than that of the control PF, in both high-frequency end (higher than 4000 Hz) and low-frequency range (2000–4000 Hz). The sound-absorption ability of PFGA continuously increased with GO content, which can only be achieved in the case of ultrathin graphene drums through plastic foaming (Figure S13A, Supporting Information). As a comparison, the prepared PF-rGO without plastic foaming only had a slight improvement on the acoustic absorption coefficient, unfulfilling the great potential of graphene.^[21,22] Besides, the overlapped absorption curves of PF-rGO5 mg and PF-rGO10 mg denote that absorption becomes saturated as coating containing increased, because that thick solid films suppressed the resonance absorption.^[21] This contrast in absorption coefficient indicates the high efficiency of ultrathin graphene drums introduced by plastic foaming.

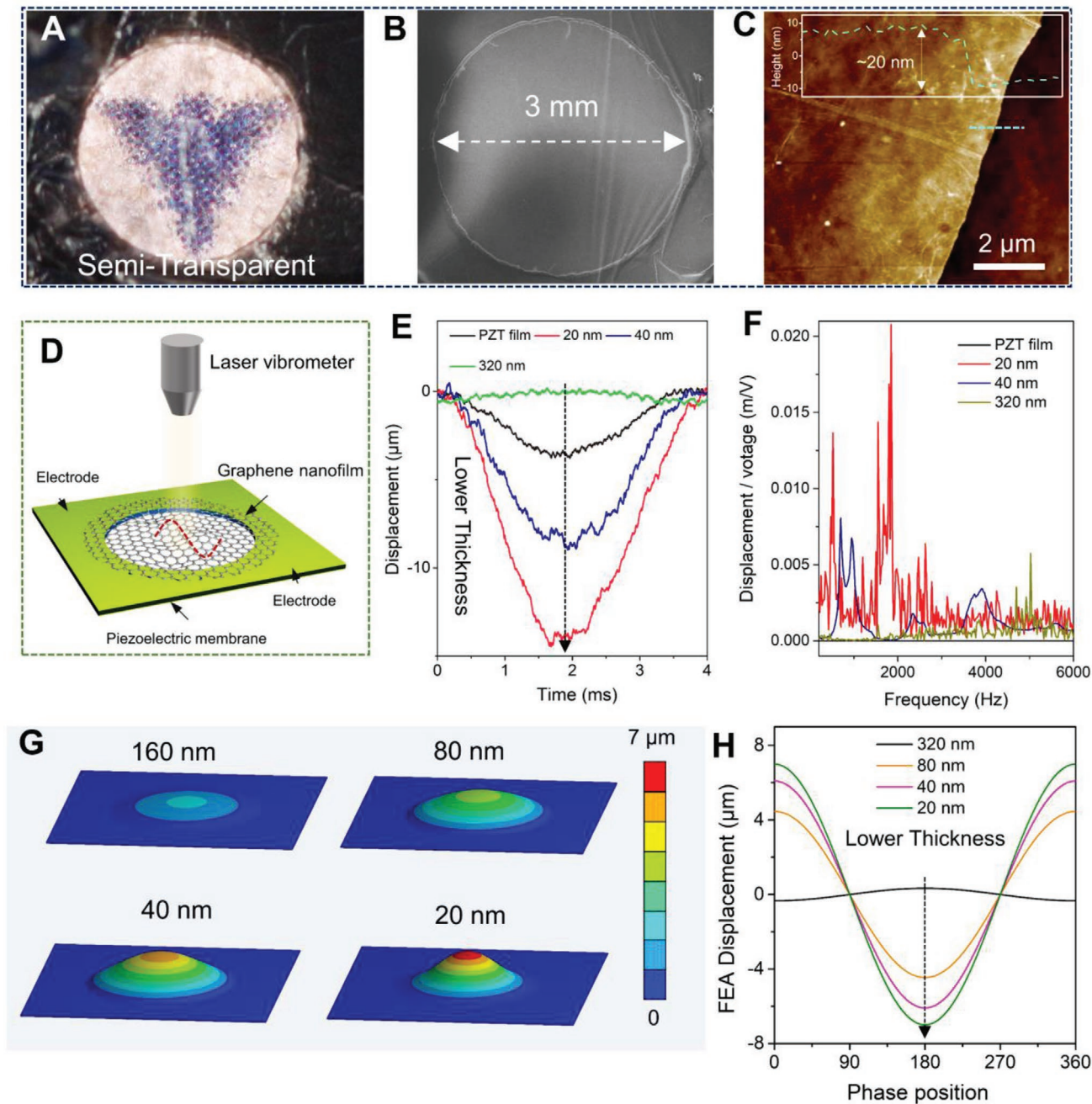


Figure 3. A) Digital photo of semitransparent graphene nanofilm. B) SEM image of graphene nanofilm suspended on a hole with diameter of 3 mm. C) AFM image of graphene nanofilm and its height measurement. D) The diagram of resonance device of ultrathin graphene drums, including hollow PVDF substrate, two-side electrodes, graphene nanofilm, and laser vibrometer. E) The vibrational displacements of pristine PZT film and ultrathin graphene drums (20, 40, and 320 nm thickness) with 200 Hz frequency input. F) The vibrational displacement per unit voltage of pristine PZT film and ultrathin graphene drums (20, 40 and, 320 nm thickness) with wide-frequency (200–6000 Hz) input. G,H) The FEA mapping (G) and calculation (H) of graphene resonances.

We also investigated the influences of foaming conditions on the sound-absorption ability of PFGAs. Figure S14A, Supporting Information, can demonstrate that the 30% N_2H_4 was the best choice to optimize the sound-absorption ability of PFGA with the thinnest wall thickness (≈ 20 nm). Larger size pores of GAs were more suitable to improve the resonance ability of graphene nanosheets, then facilitated the acoustic

absorption of PFGA (Figure S14B, Supporting Information), especially in the low-frequency region. The boundary conditions of graphene sheets on PF were controlled by the pore size of framework from 210 to 87 μm , at the same GO content (Figure S15, Supporting Information). We measured their acoustic absorption coefficient (Figure S16) and concluded that the lowered boundary size of graphene would result the

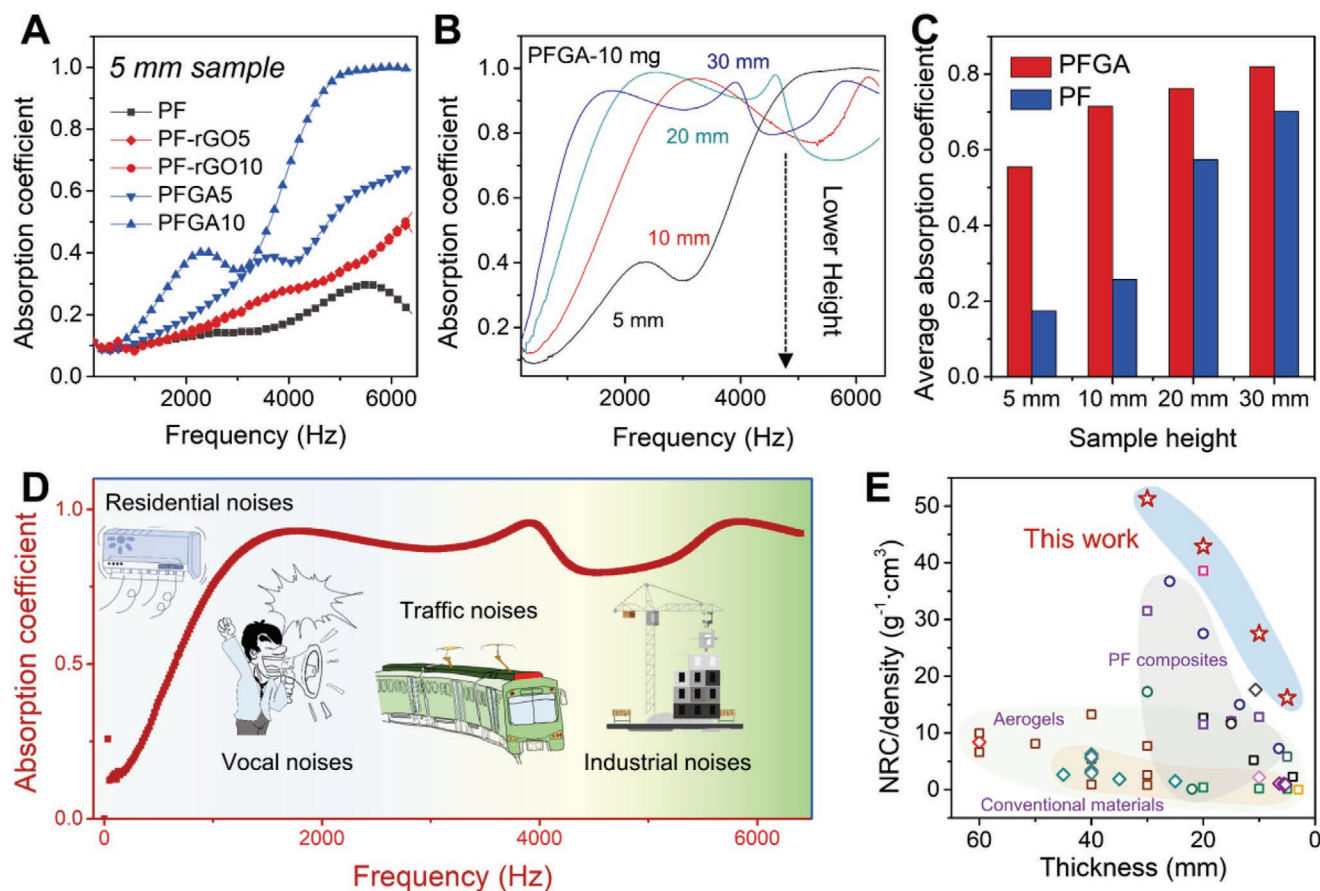


Figure 4. A) The sound-absorption coefficients of PF, PF-rGO, and PFGA at 5 mm thickness. B) The sound-absorption spectra of PFGA with different heights. C) Comparison of average absorption coefficient from 200 to 6000 Hz of PF and PFGA with different sample thickness. D) The sound absorption spectrum of PFGA covering wide frequency to include residential, vocal, traffic, and industrial noises. E) Comparison of the specific NRC between PFGA and other reported sound-absorption materials with different thickness.

decrease of acoustic absorption coefficient due to the fewer resonance units and pores.

The great mechanical robustness of PFGA guaranteed the stability of sound absorption as applied in complex deformations and environment. The absorption coefficient of PFGA still remained unchanged (Figure S13B, Supporting Information), even after 1000-cycles tensile (10% strain) or compressive tests. We also revealed that the absorption coefficient increases and absorption frequency width widens, as the thickness of PFGA increased from 5 to 30 mm (Figure 4B). At any thickness, the sound absorption coefficient of PFGA was always higher than that of PF (Figure S17A, Supporting Information). The average absorption coefficient (defined as the average value of the entire ranges) of PFGA in the wide range of 200–6000 Hz is higher than that of PF, having a peak 320% enhancement. The maximum average absorption coefficient of PFGA reaches above 0.8 from 200 to 6000 Hz (Figure 4C).

To analyze the dominated sound-absorption mechanism, we compared the absorption coefficient of PF with PFGA in different sample height (Figure S17, Supporting Information). Figure S17A, Supporting Information, demonstrated that the thicker samples whether for the PF or PFGA can dramatically increase the sound-absorption ability. From the acoustic-absorption curves of pristine PF, the absorption

coefficient can also reach the same level with PFGA from 4000 to 6000 Hz. Therefore, we conclude the acoustic frequency of 4000–6000 Hz was dominated by friction damping. Figure S17B, Supporting Information, indicated the enhanced ratio of PFGA with PF can be improved continually with the increased height at the frequency of 200–1000 Hz. From 1000 to 4000 Hz, the enhanced ratio would be decreased with the increased height, indicating more porosities in higher PF also have partial influences in this region. Therefore, the resonances of graphene drums mainly acted on low-frequency sound attenuation (200–1000 Hz) and the air-friction attenuation was the predominant mechanism at high-frequency from 4000–6000 Hz. The resonance and friction damping were collective leadership in the frequency from 1000 to 4000 Hz.

PFGA with a thickness of 30 mm exhibited a high absorption coefficient above 0.8–0.9 to cover a wide frequency range from 200 to 6000 Hz (Figure 4D). This wide absorption range basically covered the usual noise range, extending from residential, vocal to traffic and industrial noises, providing full protection of hearing health. The sound absorption efficiency can be evaluated by NRC, which is widely used in acoustic engineering field.^[35] The NRC value significantly increases from 0.19 for PFGA with thickness of 5 mm to 0.58 with thickness of 30 mm, which was invariably higher than pristine PF with

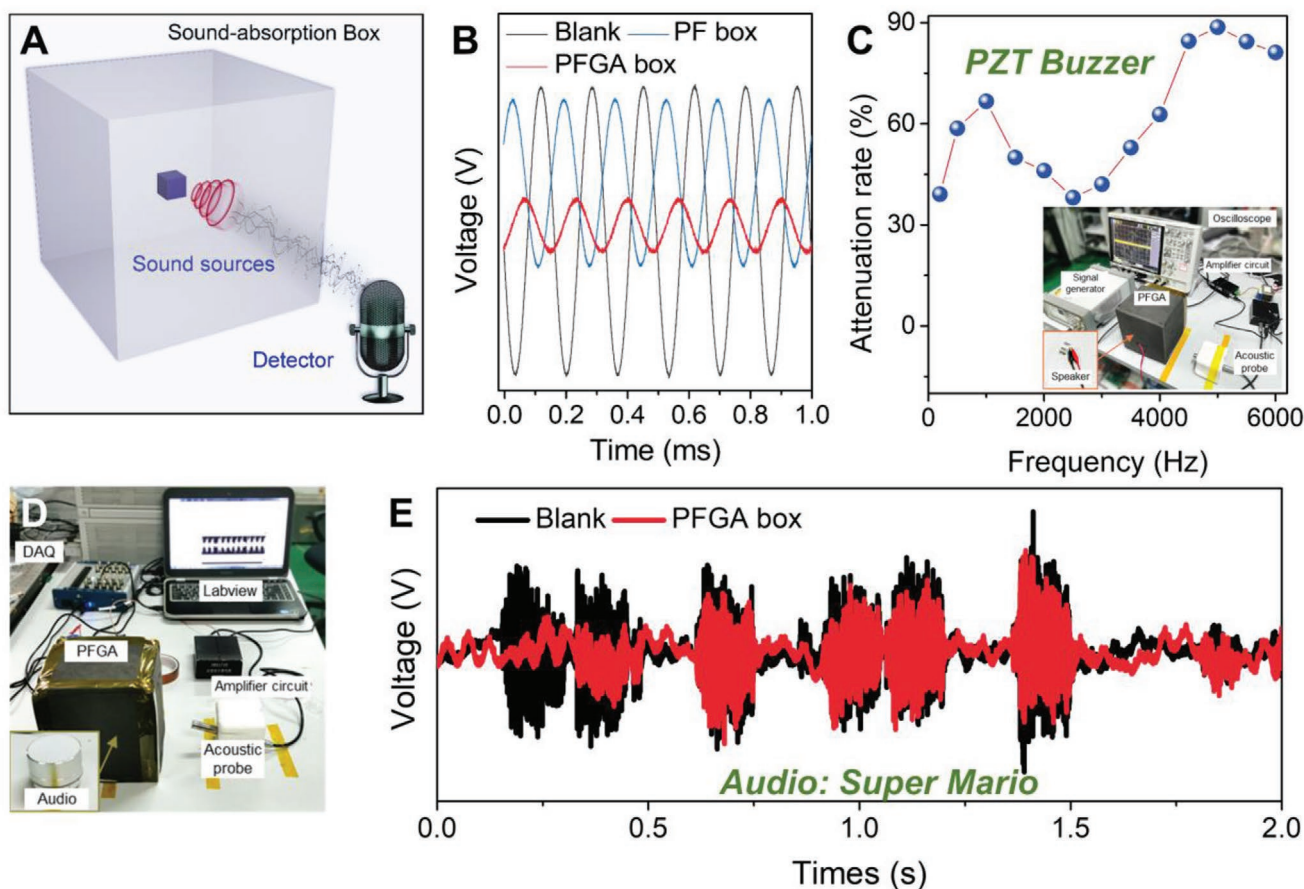


Figure 5. A) Illustration of prototype test of graphene absorber in practical applications. B) The signal intensity with or without PF and PFGA boxes with single-frequency (200 Hz) sound source by PZT buzzer. C) The attenuation rate for original sound of PFGA with different frequency sound sources. The inset is the test device, including signal generator, PFGA box, acoustic probe, amplifier circuit, and oscilloscope. D) The device of practical acoustic application with complex sound (audio source), including audio, PFGA, acoustic probe, amplifier circuit, and DAQ. E) The signals intensity with or without PFGA boxes with audio of classical melody of “Super Mario” as sound source.

same thickness (Figure S18A, Supporting Information). Moreover, the specific NRC and greater efficiency of PFGA surpassed most of the reported sound-absorption materials, such as the conventional porous materials,^[29,30,36–42] composites^[21,22,25,43–47] and ultralight aerogels^[35,48–50] (Figure 4E and Figure S18B, Supporting Information), in which air friction mechanism dominates. The superiority of PFGA in sound absorption is ascribed to the strong resonance of ultrathin graphene drums, fulfilling the overwhelming merit of graphene sheets.

We assessed the application value of PFGA absorber by the prototype tests as shown in Figure 5A. For single-frequency sound source, the alternating current frequency was converted into sound signal by PZT buzzer and the attenuated sound was detected by oscilloscope with acoustic probe after amplifier circuit (Inset of Figure 5C). The acoustic signal was greatly suppressed by PFGA box at low-frequency of 200 Hz and high-frequency of 6000 Hz, which was lower than pristine PF box (Figure 5B and Movie S2, Supporting Information). The attenuation rate, defined as the ratio of the sound intensity with and without PFGA, reached over 40% with a maximum value of 90% from 200 to 6000 Hz (Figures S6C and S19A, Supporting Information). To test the absorption efficiency of complex sound, we set up the apparatus as shown in Figure 5D. The bluetooth

speaker was adopted as source and the data acquisition card (DAQ) was used to read digital signals from amplifier acoustic frequency. For the audio of classical melody of “Super Mario” or “Metal Slug”, we found the voice intensity was obviously weakened by PFGA (Figure 5E and Figure S20, Supporting Information). The sound pressure level had a decrease than original music and the maximum reduction was changed from ≈ 68 dB to ≈ 50 dB (Figure S19B, Supporting Information). The excellent sound-absorption ability in practical environments indicates that our proposed absorber holds great promises in acoustic protection and engineering regimes.

3. Conclusion

We have developed a cellular acoustic absorber as a new assembly form to fully harness the superior resonant properties of 2D graphene in acoustic fields. We proposed the hydroplastic foaming method to solve the challenge of preparing networks of self-standing graphene nanofilms with ultrathin thickness and realized the facile and scalable production of graphene cellular acoustic absorber. The self-standing graphene membranes with ultrathin thickness serve as effectively resonance absorption

elements. These exceptional vibrational characters of graphene drums are verified by experimental results and model verification, which further demonstrated the ultimate thickness of graphene is the precondition of highly resonant amplitude. Benefiting from the synergistic dissipation of ultrathin graphene and porous cavity, the acoustic absorber exhibits remarkable enhancement by $\approx 320\%$ of average absorption from 200 to 6000 Hz. The engineering NRC of PFGA has been significantly improved with the incorporation of ultrathin graphene drums, outperforming many conventional and advanced sound absorbers. Integrating with prototype devices, we demonstrated the graphene absorber effectively attenuates the sound wave propagation in practical buzzer and audio environments. The graphene absorber provides an effective strategy to explore the superior resonance damping of 2D sheets, endows commercial foams with superior economic values, and satisfies the urgent demands for acoustic absorption from noise protection, instruments to building design, and acoustic devices.

4. Experimental Section

Fabrication of PFGA: Aqueous GO dispersions were purchased from Hangzhou Gaoxi Technology Co. Ltd. (www.gaoxitech.com). GO sheets were coated into PF by facile dipping to obtain PF-GO samples after drying. PF-GO was then immersed into the N_2H_4/H_2O (30 wt%) solution to process hydroplastic foaming.^[27] After further chemical reduction by HI/EtOH (30 vol%), the PFGA was obtained. As a comparison, PF-GO was directly treated with HI/EtOH (30 vol%) vapor to prepare chemically reduced PF-GO, named PF-rGO. The GO concentrations (1, 2, 5, and 10 mg g⁻¹) were tuned to control the content of graphene drums in PFGA, coined as PFGA 1, 2, 5, and 10.

Fabrication of Ultrathin Graphene Drum: The diluted GO dispersion (0.016 mg g⁻¹) was adopted to prepare ultrathin GO nanofilms by vacuum filtration on an anodic aluminum oxide filter membrane (Whatman Anodisc 13). The ultrathin graphene nanofilm was obtained by chemical reduction (HI vapor). The PZT PVDF film was manufactured by laser cutting (LTT-i.LASER3000) to obtain the hollow substrate. Then, the ultrathin graphene membrane was transferred onto the substrate to make graphene drum resonance devices. Signal generator (Agilent 33533A) was used to generate sinusoidal waveform stimulus and laser vibrometer (Polytec VIB-A-510) was used to collect real-time vibrational data.

Finite Element Simulation and Analysis: The theoretic analysis of graphene resonance was conducted by FEA. First, modal analysis was performed to obtain the inherent frequency of the graphene under the fixed support of hollow PVDF membrane with 3 mm diameter. Then harmonic response module was activated in which excitation frequency was applied to the mass center of the model. The modal frequencies within the twice range of the input frequency were selected, and a linear superposition of the corresponding vibration modes was calculated to achieve the peak response of the amplitude. Equation (1) is the analytic solution of single degree-of-freedom system which illustrates the calculation principle of harmonic response analysis.

$$x(t) = e^{-\zeta\omega_0 t} \left(x_0 \cos\omega_d t + \frac{\dot{x}_0 + \zeta\omega_0 x_0}{\omega_d} \sin\omega_d t \right) + \frac{G}{k} \beta e^{-\zeta\omega_0 t} \left(\sin\theta \cos\omega t + \frac{\omega_0}{\omega_d} (\zeta \sin\theta - s \cos\theta) \sin\omega t \right) + \frac{G}{k} \beta \sin(\omega t - \theta) \quad (1)$$

where ω_0 and ω_d are the inherent frequency of non-damping and damping system respectively, ω is the excitation frequency, and m , k ,

β , θ , and ζ are the mass, stiffness, dynamic amplification factor, phase displacement, and damping ratio of the system respectively, which were transferred to matrices for multi DOF system. The first part of Equation (1) refers to the initial response occurring at the beginning of its displacement time curve. The second part was consequent free vibration. They were both instant response to the forced vibration and fade away with a stable sinusoidal vibration (the last part) remained. When $s = \omega / \omega_0 \approx 1$ for harmonic response analysis, the graphene resonates, and the vibration reaches peak response of its amplitude.

Characterizations: The structure and morphology were investigated by SEM, HRSEM, HRTEM, and AFM on Hitachi S4800, JEM-2100, and VEECO Multimode systems, respectively. The compressive tests were performed on a microcomputer control electronic universal testing machine (RGWT-4000-20, REGER). The Instron Legend 2344 machine was used for tensile test. The water contact angle and electrical conductivity of PFGA were conducted with Video contact Angle analyzer (Dataphysics-OCA20) and Source meter (Keithley 2400). Transfer function method (B. K. 4206) was performed to determine the sound-absorption coefficient of materials. The acoustic probe (AWA 14600E), oscilloscope (Agilent DSO-X 4052A), DAQ (NI USB-6366) were adopted to realize the prototype tests of PFGA acoustic absorber.

Supporting Information

Supporting Information is available from the Wiley Online Library or from the author.

Acknowledgements

This work was supported by the National Natural Science Foundation of China (Nos. 52122301, 52090030, 51973191 and 51803177), National Key R&D Program of China (No. 2016YFA0200200), Hundred Talents Program of Zhejiang University (188020*194231701/113), Key research and development plan of Zhejiang Province (2018C01049), Fujian Provincial Science and Technology Major Projects (NO. 2018HZ0001-2), the Fundamental Research Funds for the Central Universities (Nos. K20200060 and 2021FZZX001-17), Key Laboratory of Novel Adsorption and Separation Materials and Application Technology of Zhejiang Province (512301-I21502), Shanxi-Zheda Institute of Advanced Materials and Chemical Engineering (2021SZ-FR004), China Postdoctoral Science Foundation (2021M702788), Postdoctoral Research Program of Zhejiang Province (ZJ2021145), and Devices of the Ministry of Education NJ2020003 (INMD-2021M06).

Conflict of Interest

The authors declare no conflict of interest.

Author Contributions

K.P. and X.L. contributed equally to this work. Z.X., Y.L., L.P., and C.G. conceived the research. K.P. and X.L. designed the experiments and analyzed the data. K.P., L.P., J.X., and J.P. did the resonance test of graphene drums. S.A. conducted with the finite element analysis. K.P. and J.P. designed the prototype test of acoustic absorber. K.P. and Z.X. wrote the manuscript and all authors provided feedback.

Data Availability Statement

The data that support the findings of this study are available from the corresponding author upon reasonable request.

Keywords

acoustic absorbers, cellular materials, graphene, ultrathin drums

Received: May 17, 2021
Revised: November 15, 2021
Published online:

- [1] R. De Alba, F. Massel, I. R. Storch, T. S. Abhilash, A. Hui, P. L. McEuen, H. G. Craighead, J. M. Parpia, *Nat. Nanotechnol.* **2016**, *11*, 741.
- [2] R. A. Barton, B. Ilic, A. M. van der Zande, W. S. Whitney, P. L. McEuen, J. M. Parpia, H. G. Craighead, *Nano Lett.* **2011**, *11*, 1232.
- [3] A. Blaikie, D. Miller, B. J. Aleman, *Nat. Commun.* **2019**, *10*, 4726.
- [4] X. G. Fan, F. Forsberg, A. D. Smith, S. Schroder, S. Wagner, H. Rodjegard, A. C. Fischer, M. Ostling, M. C. Lemme, F. Niklaus, *Nat. Electron.* **2019**, *2*, 394.
- [5] X. Xiao, S. C. Fan, C. Li, W. W. Xing, *Sensors* **2019**, *19*, 3027.
- [6] Q. Zhou, J. L. Zheng, S. Onishi, M. F. Crommie, A. K. Zettl, *Proc. Natl. Acad. Sci. U. S. A.* **2015**, *112*, 8942.
- [7] C. Y. Chen, S. Lee, V. V. Deshpande, G. H. Lee, M. Lekas, K. Shepard, J. Hone, *Nat. Nanotechnol.* **2013**, *8*, 923.
- [8] Q. X. Liang, Y. T. Wu, P. Y. Lv, J. He, F. Y. Ma, T. N. Chen, *Adv. Eng. Mater.* **2021**, *23*, 2100791.
- [9] H. Ryoo, W. Jeon, *Appl. Phys. Lett.* **2018**, *113*, 121903.
- [10] S. A. Cummer, J. Christensen, A. Alu, *Nat. Rev. Mater.* **2016**, *1*, 16001.
- [11] J. Mei, G. C. Ma, M. Yang, Z. Y. Yang, W. J. Wen, P. Sheng, *Nat. Commun.* **2012**, *3*, 756.
- [12] X. W. Li, X. Yu, J. W. Chua, H. P. Lee, J. Ding, W. Zhai, *Small* **2021**, *17*, 2100336.
- [13] X. H. Zhang, Z. G. Qu, H. Wang, *iScience* **2020**, *23*, 101110;
- [14] Z. Zhou, S. Huang, D. Li, J. Zhu, Y. Li, *Natl. Sci. Rev.* **2021**, <https://doi.org/10.1093/nsr/nwab171>.
- [15] F. Bucciarelli, G. P. M. Fierro, M. Meo, *Appl. Acoust.* **2019**, *146*, 134.
- [16] Z. Q. Liu, J. X. Zhan, M. Fard, J. L. Davy, *Appl. Acoust.* **2017**, *121*, 25.
- [17] H. Q. Duan, X. M. Shen, Q. Yin, F. Yang, P. F. Bai, X. N. Zhang, M. Pan, *Appl. Acoust.* **2020**, *166*, 107322.
- [18] H. S. Kim, P. S. Ma, B. K. Kim, S. R. Kim, S. H. Lee, *J. Sound. Vib.* **2019**, *460*, 114884.
- [19] A. Keskekler, O. Shoshani, M. Lee, H. S. J. van der Zant, P. G. Steeneken, F. Alijani, *Nat. Commun.* **2021**, *12*, 1099.
- [20] J. C. Trevor, D. A. Peter, *Acoustic Absorbers and Diffusers: Theory, Design, and Application*, Spon Press, London, UK **2004**.
- [21] M. J. Nine, M. Ayub, A. C. Zander, D. N. H. Tran, B. S. Cazzolato, D. Losic, *Adv. Funct. Mater.* **2017**, *27*, 1703820.1.
- [22] J. Lee, I. Jung, *Appl. Acoust.* **2019**, *151*, 10.
- [23] M. Rapisarda, G. P. M. Fierro, M. Meo, *Sci. Rep.* **2021**, *11*, 10572.
- [24] B. Lu, L. X. Lv, H. S. Yang, J. Gao, T. Xu, G. Q. Sun, X. T. Jin, C. X. Shao, L. T. Qu, J. Yang, *J. Mater. Chem. A* **2019**, *7*, 11423.
- [25] L. Liu, Y. J. Chen, H. Z. Liu, H. U. Rehman, C. Chen, H. M. Kang, H. Li, *Soft Matter* **2019**, *15*, 2269.
- [26] C. Simon-Herrero, N. Peco, A. Romero, J. L. Valverde, L. Sanchez-Silva, *Appl. Acoust.* **2019**, *156*, 40.
- [27] K. Pang, X. Song, Z. Xu, X. T. Liu, Y. J. Liu, L. Zhong, Y. X. Peng, J. X. Wang, J. Z. Zhou, F. X. Meng, J. Wang, C. Gao, *Sci. Adv.* **2020**, *6*, eabd4045.
- [28] L. B. Wang, C. Z. Ma, J. H. Wu, *Appl. Acoust.* **2021**, *179*, 108025.
- [29] U. Berardi, G. Iannace, *Appl. Acoust.* **2017**, *115*, 131.
- [30] J. Z. Wang, Q. B. Ao, J. Ma, X. T. Kang, C. Wu, H. P. Tang, W. D. Song, *Appl. Acoust.* **2019**, *145*, 431.
- [31] H. Q. Li, N. Zhang, X. D. Fan, J. X. Gong, J. F. Zhang, X. M. Zhao, *Appl. Acoust.* **2020**, *161*, 107081.
- [32] H. L. Gao, Y. B. Zhu, L. B. Mao, F. C. Wang, X. S. Luo, Y. Y. Liu, Y. Lu, Z. Pan, J. Ge, W. Shen, Y. R. Zheng, L. Xu, L. J. Wang, W. H. Xu, H. A. Wu, S. H. Yu, *Nat. Commun.* **2016**, *7*, 12920.
- [33] Y. P. Wu, N. B. Yi, L. Huang, T. F. Zhang, S. L. Fang, H. C. Chang, N. Li, J. Oh, J. A. Lee, M. Kozlov, A. C. Chipara, H. Terrones, P. Xiao, G. K. Long, Y. Huang, F. Zhang, L. Zhang, X. Lepro, C. Haines, M. D. Lima, N. P. Lopez, L. P. Rajukumar, A. L. Elias, S. M. Feng, S. J. Kim, N. T. Narayanan, P. M. Ajayan, M. Terrones, A. Aliev, P. F. Chu, et al., *Nat. Commun.* **2015**, *6*, 6141.
- [34] X. L. Zhao, W. Q. Yao, W. W. Gao, H. Chen, C. Gao, *Adv. Mater.* **2017**, *29*, 1701482.
- [35] C. Jia, L. Li, Y. Liu, B. Fang, H. Ding, J. N. Song, Y. B. Liu, K. J. Xiang, S. Lin, Z. W. Li, W. J. Si, B. Li, X. Sheng, D. Z. Wang, X. D. Wei, H. Wu, *Nat. Commun.* **2020**, *11*, 3732.
- [36] Y. Na, G. Cho, *Fibers Polym.* **2010**, *11*, 782.
- [37] E. Taban, A. Tajpoor, M. Faridan, S. E. Samaei, M. H. Beheshti, *Acoust. Aust.* **2019**, *47*, 67.
- [38] T. Yang, L. Z. Hu, X. M. Xiong, M. Petru, M. T. Noman, R. Mishra, J. Militky, *Sustainability* **2020**, *12*, 8477.
- [39] F. S. Han, G. Seiffert, Y. Y. Zhao, B. Gibbs, *J. Phys. D: Appl. Phys.* **2003**, *36*, 294.
- [40] X. W. Li, X. Yu, W. Zhai, *Adv. Mater.* **2021**, *33*, 2104552.
- [41] M. K. Ozturk, F. B. Nergis, C. Candan, *Polym. Adv. Technol.* **2018**, *29*, 1255.
- [42] Y. X. Wang, J. W. Guo, Y. Fang, X. Zhang, H. Y. Yu, *Adv. Eng. Mater.* **2021**, *23*, 2100563.
- [43] S. C. Pinto, P. A. A. P. Marques, M. Vesenjak, R. Vicente, L. Godinho, L. Krstulovic-Opara, I. Duarte, *Metals* **2019**, *9*, 1214.
- [44] Y. Wu, X. Y. Sun, W. Wu, X. Liu, X. Y. Lin, X. Shen, Z. Y. Wang, R. K. Y. Li, Z. Y. Yang, K. T. Lau, J. K. Kim, *Composites, Part A* **2017**, *102*, 391.
- [45] S. M. Chen, Y. Jiang, *Polym. Compos.* **2018**, *39*, 1370.
- [46] J. H. Oh, H. R. Lee, S. Umrao, Y. J. Kang, I. K. Oh, *Carbon* **2019**, *147*, 510.
- [47] C. M. Wu, M. H. Chou, *Eur. Polym. J.* **2016**, *82*, 35.
- [48] Y. Si, J. Y. Yu, X. M. Tang, J. L. Ge, B. Ding, *Nat. Commun.* **2014**, *5*, 5802.
- [49] F. Xu, S. Y. Zhang, G. G. Wang, D. Q. Zhao, J. W. Feng, B. L. Wang, X. D. He, *Adv. Mater. Interfaces* **2021**, *8*, 2100183.
- [50] L. T. Cao, Y. Si, Y. Y. Wu, X. Q. Wang, J. Y. Yu, B. Ding, *Nanoscale* **2019**, *11*, 2289.